First-principles analysis of MoS_2/Ti_2C and MoS_2/Ti_2CY_2 (Y = F and OH) all-2D semiconductor/metal contacts

Li-Yong Gan,[1] Yu-Jun Zhao,[2] Dan Huang,[3] and Udo Schwingenschlögl[1,*]

[1]*Physical Sciences and Engineering Division, King Abdullah University of Science and Technology (KAUST), Thuwal 23955-6900, Kingdom of Saudi Arabia*

[2]*Department of Physics, South China University of Technology, Guangzhou 510640, People's Republic of China*

[3]*Department of Physics and Electronic Sciences, Hunan University of Arts and Science, Changde 415000, People's Republic of China*

(Received 17 February 2013; published 13 June 2013)

First-principles calculations are used to explore the geometry, bonding, and electronic properties of MoS_2/Ti_2C and MoS_2/Ti_2CY_2 (Y = F and OH) semiconductor/metal contacts. The structure of the interfaces is determined. Strong chemical bonds formed at the MoS_2/Ti_2C interface result in additional states next to the Fermi level, which extend over the three atomic layers of MoS_2 and induce a metallic character. The interaction in MoS_2/Ti_2CY_2, on the other hand, is weak and not sensitive to the specific geometry, and the semiconducting nature thus is preserved. The energy level alignment implies weak and strong n-type doping of MoS_2 in MoS_2/Ti_2CF_2 and $MoS_2/Ti_2C(OH)_2$, respectively. The corresponding n-type Schottky barrier heights are 0.85 and 0.26 eV. We show that the MoS_2/Ti_2CF_2 interface is close to the Schottky limit. At the $MoS_2/Ti_2C(OH)_2$ interface, we find that a strong dipole due to charge rearrangement induces the Schottky barrier. The present interfaces are well suited for application in all-two-dimensional devices.

DOI: 10.1103/PhysRevB.87.245307 PACS number(s): 73.20.−r, 73.21.Ac, 73.22.−f, 73.30.+y

Heterostructures of semiconductors and metals play a key role in modern electronic and photonic devices, being more crucial than the semiconductors themselves.[1,2] Coherent and passivated interfaces, particularly, govern the properties of high-mobility transistors, solid state lasers, light-emitting devices, and solar cells, since interfacial defects can severely degrade the performance.[3] While single-crystal semiconductor-metal contacts are well controlled in Si-based technology,[4] implementation of low-dimensional heterojunctions is enormously challenging, though very important for achieving advanced functionalities.[3,5] Single-layer transition metal dichalcogenides (TMDCs), especially monolayer MoS_2, exhibit many promising prospects in electronics and optoelectronics due to their exotic electronic, optical, mechanical, chemical, and thermal properties, compared with their bulk counterparts, especially MoS_2.[6–11] The direct band gap of MoS_2 enables applications in logic transistors,[1] photodetectors, and electroluminescent devices.[12,13] The band gap of 1.75–1.90 eV[11,14–16] lies just in the visible energy range and thus is suitable for photocatalysis.[17,18] However, there are still limitations in TMDC electronic devices, for example, the relatively high effective mass of the carriers and low carrier mobility,[19] hampering high-performance applications.

Integration of MoS_2 with other two-dimensional (2D) materials to form 2D hybrid systems can give rise to remarkable electronic properties, which attracts increasing interest.[6,20–24] MoS_2 growth on graphene increases the electronic conductivity, as well as electrochemical and photochemical performances.[20,21] Field-effect transistors with high switching ratio have been fabricated using two independently controlled graphene layers separated by thin MoS_2 or hexagonal boron nitride.[6] Combining TMDCs with other 2D layered materials, therefore, is viable and promising for vertical heterostructures and hybrid all-2D devices.[7,25] However, for this purpose, it is vital to understand the electronic structures of hybrid systems in detail.

Very recently, new families of 2D graphene-like carbides and carbonitrides, so-called *MX*enes (M = Ti, Sr, V, Cr, Ta, Nb, Zr, Mo, Hf; X = C, N, or both), have been synthesized from layered $M_{n+1}AX_n$ (n = 1, 2, and 3),[26,27] in which A represents elements mainly from groups IIIA and IVA. These materials display not only structural similarity to graphene but also show a high electrical conductivity,[28,29] which may allow to enhance TMDC electronic devices by the formation of heterojunctions with *MX*enes. It is important to explore the physics of contacts between TMDCs and *MX*enes for various reasons. In general, the behavior of semiconductor-metal interfaces is a long-standing fundamental issue. It has been shown that the nature of the contact between MoS_2 and metal electrodes depends on the specific transition metal incorporated.[5] In particular, the effect of the reduced dimensionality in 2D systems is difficult to predict. Technologically, the potential of TMDCs and *MX*enes in electronic and photonic devices is vital to be understood in detail.

It was found that the lattice constant of a Ti_2C monolayer, a prototypical *MX*ene, is 3.076 Å,[30] which is very close to the value of MoS_2.[31,32] The analogous hexagonal lattices offer the possibility to form coherent interfaces with slight lattice mismatch, which gives rise to a prototypical system to investigate the basic behavior of all-2D heterojunctions. However, so far, neither experimental nor theoretical studies have been conducted on this promising class of interfaces. Thus, the present work addresses interfaces between the nonmagnetic semiconductor MoS_2 and the ferromagnet Ti_2C,[30] as well as its derivatives [i.e., the nonmagnetic metals[33] Ti_2CY_2 (Y = F and OH)], to explore the potential of these new hybrid systems in all-2D electronic and optoelectronic devices. It is found that metallic features appear in MoS_2 in contact with Ti_2C, while different degrees of n-type doping are realized upon interface formation with Ti_2CY_2. This is highly desirable to achieve hybrid all-2D electronic and optoelectronic devices, such as diode lasers.[7]

 ©2013 American Physical Society

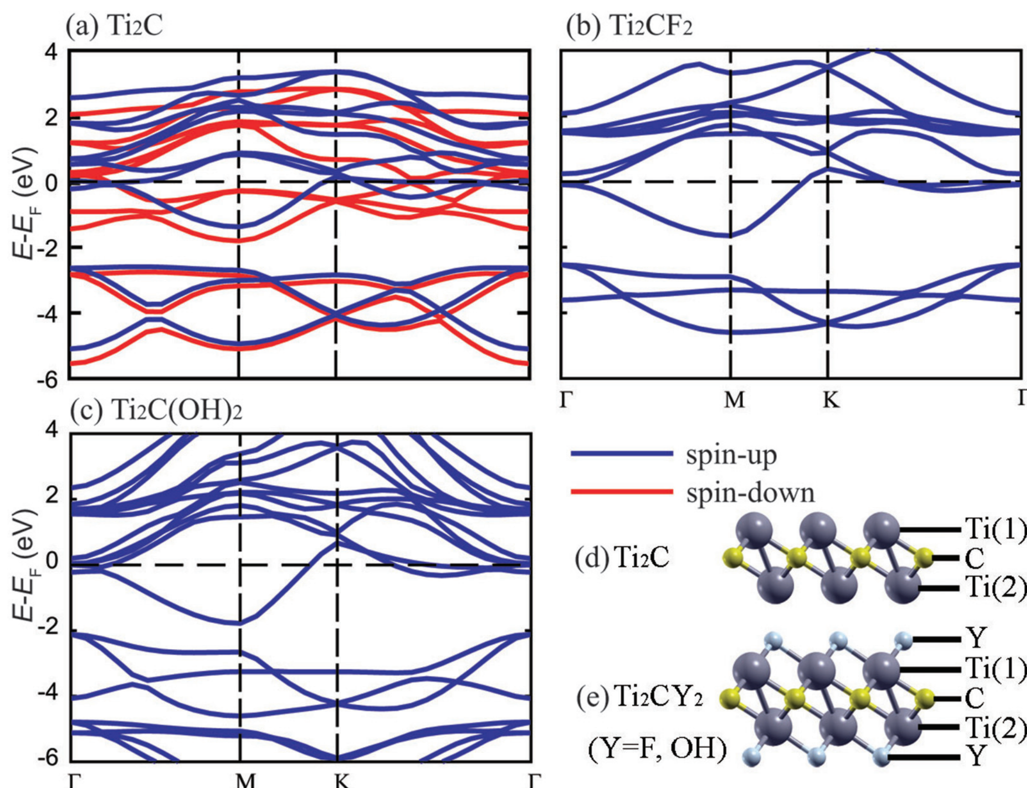

FIG. 1. (Color online) Spin-polarized band structures of (a) free-standing Ti_2C, (b) Ti_2CF_2, and (c) $Ti_2C(OH)_2$. Side views of Ti_2C and Ti_2CY_2 are given in panels (d) and (e), respectively.

First-principles calculations are performed using the Vienna *Ab initio* Simulation Package with the spin-polarized Perdew, Burke, and Ernzerhof (PBE) generalized gradient approximation functional.[34–38] A cutoff energy of 500 eV and a Γ-centered $25 \times 25 \times 1$ k-mesh are used. Geometry optimization is continued until the residual forces are less than 0.02 eV/Å, and a dipole correction[36] is applied due to the asymmetric layer arrangement. Because of the absence of strong bonding, a damped van der Waals (vdW) correction (DFT-D2)[39] is adopted to consider the nonbonding forces.

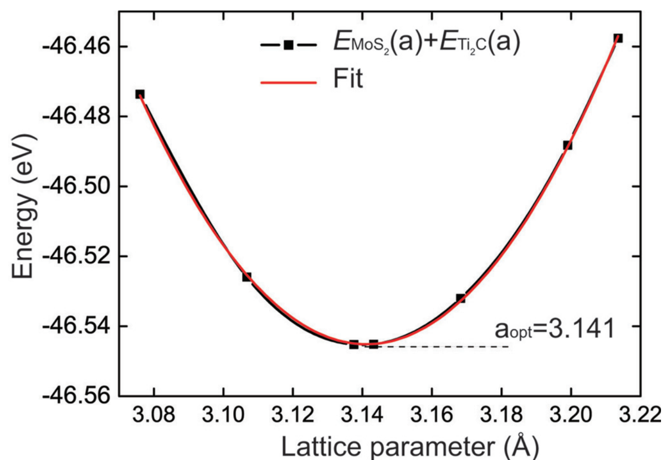

FIG. 2. (Color online) Lattice parameter optimization of the MoS_2/Ti_2C interface.

As a starting point, the electronic properties of the four free-standing monolayers, MoS_2, Ti_2C, Ti_2CF_2, and $Ti_2C(OH)_2$ are studied. The MoS_2 monolayer is found to be a semiconductor with a direct band gap of 1.69 eV with and without consideration of the vdW correction. Both the conduction band minimum (CBM) and the valence band maximum (VBM) are located at the K point, consistent with previous studies.[11,14–16] Ti_2C is magnetic with a total magnetic moment of 1.85 μ_B per unit cell, where the spin up and down bands both cross the Fermi level. For Ti_2CY_2 it is found that a configuration with Y located above a hollow site pointing directly toward Ti [Fig. 1(e)] is energetically preferable. The calculated band structures [Figs. 1(b) and 1(c)] indicate metallicity with degenerate spin channels,[33] making Ti_2C and Ti_2CY_2 potentially applicable in electrical devices. The calculated work function of Ti_2C is 3.98 eV (both with and without vdW correction), which is increased by F saturation but decreased by OH groups. Surprisingly, the calculated work function of $Ti_2C(OH)_2$ is only 1.65 eV (1.70 eV using DFT-D2).[40]

The relaxed lattice constants of Ti_2C and MoS_2 are 3.076 Å and 3.181 Å, respectively, including around 3% lattice mismatch. The optimal lattice constant of the MoS_2/Ti_2C interface is obtained by minimizing the sum of the total energies of Ti_2C and MoS_2 (3.07 ∼ 3.21 Å), as shown in Fig. 2, yielding 3.141 Å, which is adopted for MoS_2/Ti_2CY_2. There are in total six stacking patterns for MoS_2 on Ti_2C and Ti_2CY_2. Only $MoS_2/Ti_2C(OH)_2$ is shown in Fig. 3: The atop-I and -II patterns have S above Ti(1) and Mo above C and Ti(2), respectively; patterns fcc-I and -II have S above Ti(2) and

TABLE I. Cohesive energy E_{coh}, optimized interlayer distance d between MoS_2 and Ti_2C and Ti_2CY_2 (Y = F and OH), and work function Φ_M.

		PBE			DFT-D2		
System	Pattern	E_{coh} (eV)	d (Å)	Φ_M (eV)	E_{coh} (eV)	d (Å)	Φ_M (eV)
Ti_2C				3.98			3.98
MoS_2/Ti_2C	atop-I	– 0.66	2.50	4.69	– 0.84	2.48	4.69
	atop-II	– 0.55	2.50	4.77	– 0.83	2.45	4.65
	fcc-I	– 1.13	1.67	4.60	– 1.62	1.64	4.53
	fcc-II	– 0.65	1.89	4.79	– 1.00	1.85	4.80
	hcp-I	– 0.48	1.81	4.89	– 0.85	1.75	4.85
	hcp-II	– 1.04	1.65	4.56	– 1.45	1.63	4.56
Ti_2CF_2				4.85			4.82
MoS_2/Ti_2CF_2	atop-I	0.09	3.09	4.88	– 0.01	3.08	4.84
	atop-II	0.09	3.05	4.87	– 0.02	2.83	4.80
	fcc-I	0.09	3.37	4.94	0.02	3.16	4.90
	fcc-II	0.09	3.39	4.93	0.02	3.19	4.90
	hcp-I	0.10	3.03	4.91	– 0.02	2.86	4.89
	hcp-II	0.09	3.06	4.91	– 0.02	2.75	4.87
$Ti_2C(OH)_2$				1.65			1.70
$MoS_2/Ti_2C(OH)_2$	atop-I	– 0.10	2.19	4.04	– 0.25	2.14	4.04
	atop-II	– 0.09	2.20	4.03	– 0.25	2.15	4.03
	fcc-I	– 0.13	2.32	4.01	– 0.25	2.32	4.01
	fcc-II	– 0.13	2.29	4.01	– 0.25	2.29	4.01
	hcp-I	– 0.09	2.19	4.03	– 0.24	2.18	4.04
	hcp-II	– 0.09	2.21	4.02	– 0.24	2.16	4.03

Mo above Ti(1) and C, respectively; patterns hcp-I and -II have S above C and Mo above Ti(1) and Ti(2), respectively. The cohesive energy of the interface systems is defined as $E_{coh} = E_{IS} - E_M - E_{sub}$, where E_{IS}, E_M, and E_{sub} represent the total energies of the hybrid system, MoS_2 monolayer, and substrates, respectively. The cohesive energies, interlayer spacings, and work functions of the individual and hybrid systems are listed in Table I.

According to Table I, MoS_2 interacts strongly with Ti_2C. The PBE calculated energies and interlayer spacings suggest chemical bond formation with significant configuration dependence. The order of stability for MoS_2/Ti_2C is: hcp-I < atop-II < fcc-II < atop-I < hcp-II < fcc-I. For MoS_2 on the two Y saturated surfaces, the PBE results indicate that the interaction is rather weak and not sensitive to the specific arrangements. Specifically, formation of the MoS_2/Ti_2CF_2 interface is endothermic and all interlayer distances are larger than 3 Å in the six arrangements. The weak interaction in MoS_2/Ti_2CY_2 is comparable to that in the graphene/MoS_2[41] and some graphene/metal systems.[42,43] In order to demonstrate the effects of vdW interaction, the cohesive energies and optimized interlayer spacings obtained under inclusion of the vdW correction are also listed in Table I. In MoS_2/Ti_2C, the vdW interaction increases the cohesive energy by more than one third but does not alter the interlayer spacing too much. In MoS_2/Ti_2CY_2, the cohesive energy is twice the PBE value and the interlayer spacing is much smaller. This significant difference between the PBE and DFT-D2 results indicates that the vdW interaction plays an extremely important role in the three examined interfaces, especially in MoS_2/Ti_2CY_2. Therefore, in the following, all electronic properties are calculated including the vdW correction.

According to the energetics, the interfaces can be divided into two classes: chemisorption of MoS_2 on Ti_2C and physisorption on Ti_2CY_2. We first focus on the first class. The density of states (DOS) and charge density difference of MoS_2 in the energetically favorable pattern of MoS_2/Ti_2C (fcc-I) is addressed in Fig. 4 to explore the electronic structure variations induced by the interface. It can be seen that the strong interactions at the interface modify the electronic properties

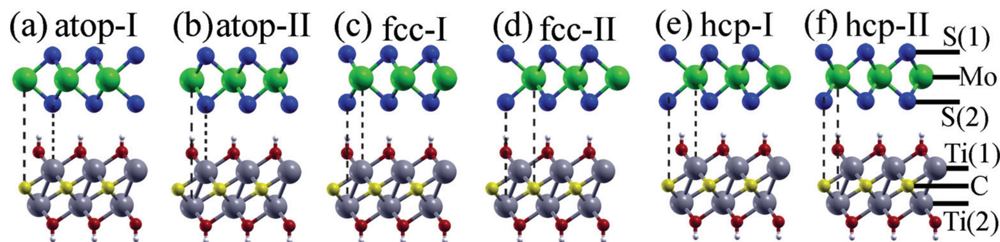

FIG. 3. (Color online) Side views of the six nonequivalent stacking patterns of the $MoS_2/Ti_2C(OH)_2$ interface. The green, blue, gray, yellow, red, and white balls represent Mo, S, Ti, C, O, and H atoms, respectively.

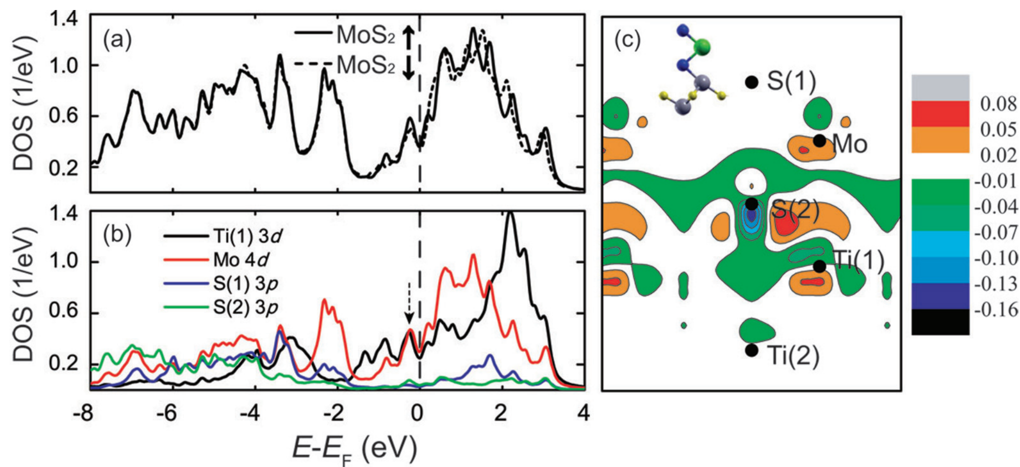

FIG. 4. (Color online) (a) Spin-polarized total and (b) partial DOSs of adsorbed MoS_2 and (c) charge density difference for MoS_2/Ti_2C for pattern fcc-I [inset in panel (c)]. The atomic positions are marked by solid circles. Arrows in panel (a) indicate the two spin channels. The dashed arrow in panel (b) highlights the metal-induced states in MoS_2.

remarkably. Tiny magnetic features appear that are ascribed to the unsaturated Ti(1) $3d$ dangling bonds present in Ti_2C. The partial DOS is plotted only for one spin channel of the S(1), Mo, S(2), and Ti(1) atoms, together with the charge density difference to investigate the bonding mechanism in MoS_2/Ti_2C. A distinct overlap between the Ti(1) $3d$, Mo $4d$, and S(2) $3p$ orbitals can be seen near the Fermi level, suggesting strong hybridization upon interface formation. Additionally, metal-induced states[44] appear in the partial DOS of all three atomic layers of MoS_2, especially the Mo layer, as indicated by the dashed arrow in Fig. 4(b). The states at the Ti_2C/MoS_2 interface extend over the three atomic layers of MoS_2, namely, 3.25 Å. Therefore, a metallic character replaces the semiconducting nature of MoS_2. This finding suggests that deposition of Ti_2C significantly increases the conductivity of a MoS_2 monolayer. As is shown in Fig. 4(c), charge is depleted from the Ti $3d$ dangling bond of bare Ti_2C[30] and the S(2) p_z orbital, while it accumulates in the S(2) and Ti(1) bond region. The strong S(2)-Ti bonds formed at the interface weaken the Mo-S(2) bonds in the MoS_2 layer according to the bond order conservation concept,[45] inducing a polarized Mo d orbital, which is similar to a dangling bond. We note that a second MoS_2 layer added to the system remains semiconducting with an indirect band gap, because the separation of the two MoS_2 layers is 3.0 Å, so the metallic states, as shown in Fig. 4(b), cannot persist.

In contrast, the interaction between MoS_2 and Ti_2CY_2 is rather weak and thus interpreted as physisorption. In all the studied systems, the electronic properties of Ti_2CY_2 are hardly changed, resulting in metallicity in the hybrid structures. Both the PBE and DFT-D2 functionals give similar values for the work function: ~4.90 eV in MoS_2/Ti_2CF_2 and ~4.02 eV in $MoS_2/Ti_2C(OH)_2$. In addition, these values are independent of the specific arrangement. Figure 5 demonstrates the changes in the electronic structure of physisorbed MoS_2 upon formation of the interfaces. For both MoS_2/Ti_2CF_2 and $MoS_2/Ti_2C(OH)_2$ we select only one structure as a prototype, namely, MoS_2/Ti_2CF_2 atop-II and $MoS_2/Ti_2C(OH)_2$ atop-I, due to their similar energetics and electronic properties. The conduction and valence bands show that the adsorbed MoS_2 preserves mostly its character, unlike the case of MoS_2/Ti_2C where metallic features appear. Both the CBM and VBM are still located at the K point. However, the two bands are cut into pieces by the interaction between MoS_2 and Ti_2CF_2. Since the interaction is much stronger in $MoS_2/Ti_2C(OH)_2$ than in MoS_2/Ti_2CF_2, more pieces are obtained in the former case. Additionally, the interaction enhances the band gaps by 0.13 and 0.16 eV, respectively. As is shown in Fig. 5(c), these increments are mainly ascribed to the lattice compression of 1.3%.[46] Taking the vacuum level V_∞ as reference value, we can align the energy levels of the two examined hybrid systems to get detailed insight into the CBM and VBM shifts in the MoS_2 upon physisorption, as illustrated in Fig. 5(e). First, the lattice compression induces VBM and CBM shifts by 0.15 and 0.29 eV, respectively. With respect to the band structure of the compressed MoS_2, tiny shifts are found in MoS_2/Ti_2CY_2. It can be seen that the Fermi level in MoS_2/Ti_2CF_2 is only 0.06 eV higher than the midgap [i.e., (CBM + VBM)/2], suggesting a rather weak n-type doping in physisorbed MoS_2, while it is much closer to the CBM in $MoS_2/Ti_2C(OH)_2$, indicating a strong n-type doping. Therefore, the results demonstrate an effective approach to realize n-type doping of MoS_2 by 2D material contacts. For photosplitting of water, electron transfer to a proton to form atomic H is a critical step. The demonstrated strong n-type doping of MoS_2 and upshift of the VBM support the electron transfer and therefore promote the process.

One of the most important features of metal-semiconductor contacts is the Schottky barrier height. The barrier is an intrinsic property of the interface and defined by the relative alignment of the metal's Fermi level and the semiconductor's VBM (p-type barrier, $\Phi_{B,p}$) or CBM (n-type barrier, $\Phi_{B,n}$). Figure 5(d) shows that the n-type Schottky barrier height is calculated to be 0.85 and 0.26 eV in MoS_2/Ti_2CF_2 and $MoS_2/Ti_2C(OH)_2$, respectively. In order to understand the details of the bonding mechanism in the two examined physisorbed systems, the plane-averaged charge density difference $\Delta\rho(z)$ is plotted in Fig. 6, visualizing the

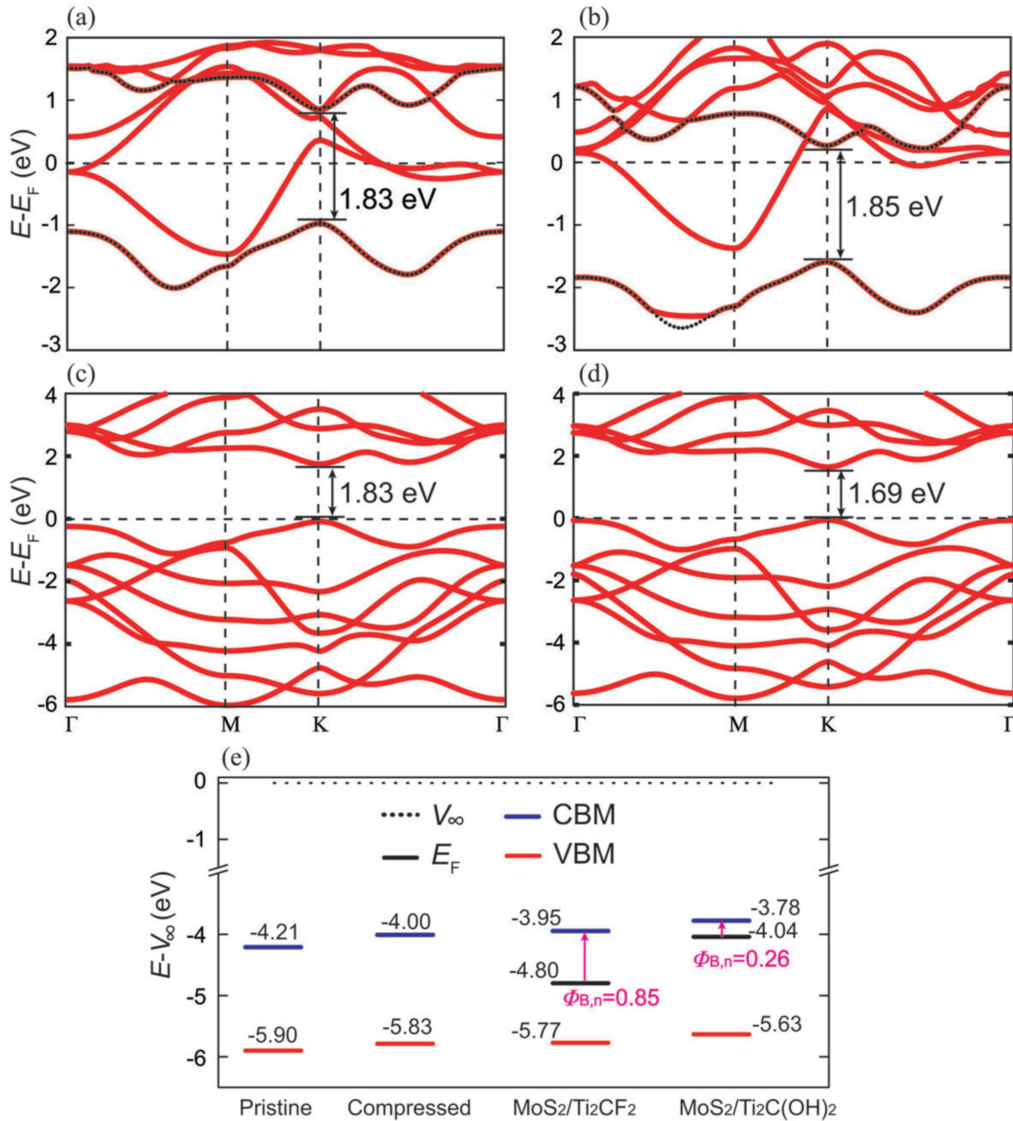

FIG. 5. (Color online) Band structures of (a) MoS_2/Ti_2CF_2 atop-II, (b) $MoS_2/Ti_2C(OH)_2$ atop-I, and (c) compressed (d) pristine MoS_2. The MoS_2-derived conduction and valence bands in the two hybrid systems are depicted by black dotted curves. (e) The energy level alignment of adsorbed MoS_2 compared with the pristine material, referring to the vacuum level (V_∞). The n-type Schottky barrier heights $\Phi_{B,n}$ are indicated by pink fonts.

charge redistribution at the interfaces. The induced charge transfer q is estimated by integrating $\Delta\rho(z)$ from $z = 0$ to 40 Å. Charge accumulation is found at both interfaces. The results imply that a weak interaction does not preclude charge transfer between MoS_2 and Ti_2CY_2, similar to the graphene/metal physisorption.[42,43,47] The charge redistribution in $MoS_2/Ti_2C(OH)_2$ is much more pronounced, with q more than 40 times larger than in MoS_2/Ti_2CF_2, resulting in a much stronger interaction, higher n-type doping of the MoS_2, and more pronounced Fermi level shift.

As shown in Fig. 6, charge transfer at the MoS_2/Ti_2CF_2 interface is negligible and since the equilibrium distance is as large as 3.0 Å, the interface can be understood by the Schottky limit,[48] in which the n-type barrier is given by the difference between the work function of the metal (Φ_M) and the electron affinity of the semiconductor (χ_s). The work function of Ti_2CF_2 is 4.82 eV and χ_s is 4.00 eV, since the adsorbed MoS_2 is compressed. This leads to $\Phi_{B,n} = 0.82$ eV, which is only 0.03 eV smaller than the value derived from the band structure, inferring a rather weakly pinned Fermi level (pinning parameter close to 1). In $MoS_2/Ti_2C(OH)_2$, however, the situation is more complicated. Figure 7 shows the plane-averaged electrostatic potential along the interface normal. We observe a discontinuity of 2.50 eV between the vacuum levels on the MoS_2 and $Ti_2C(OH)_2$ sides. This interface dipole of $\mu_{IS} = 2.50$ eV is induced by charge rearrangement upon interface formation. The charge rearrangement modifies the n-type barrier from the Schottky–Mott condition to $\Phi_{Bn} = \Phi_M + \mu_{IS} - \chi_s$,[49] giving a value of 0.20 eV, which is very close to the band structure result of 0.26 eV. This fact suggests that the barrier is mainly due to the interface dipole. The small deviation may result from other factors such as the weak hybridization between the H s and S p orbitals.[50]

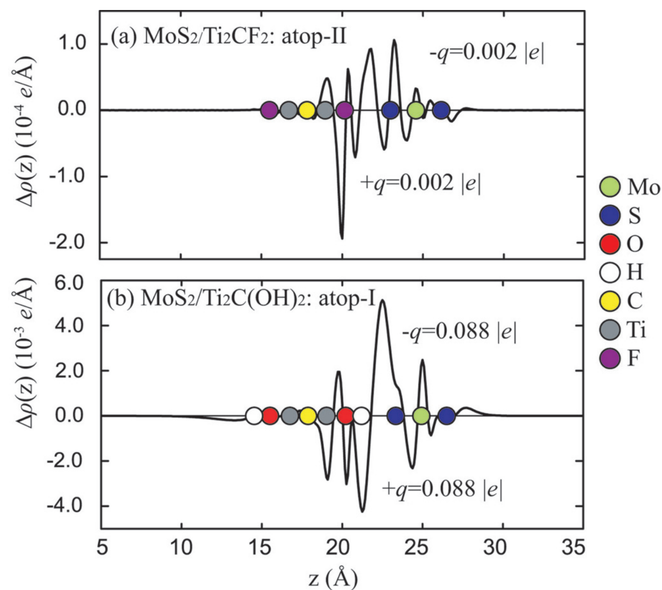

FIG. 6. (Color online) Plane-averaged electron density difference, $\Delta\rho(z)$, for the systems (a) MoS_2/Ti_2CF_2 atop-II and (b) $MoS_2/Ti_2C(OH)_2$ atop-I. The positions of the atoms are indicated by solid circles, and q is the charge transfer calculated by integrating $\Delta\rho(z)$ over the full z range.

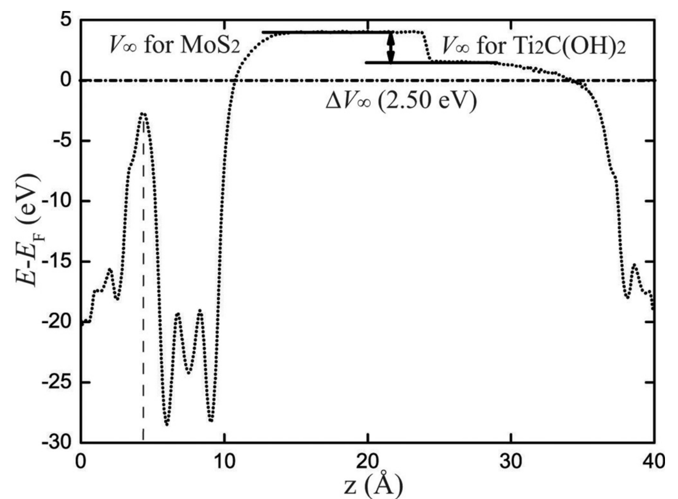

FIG. 7. Plane-averaged electrostatic potential (dotted line) along the interface normal of $MoS_2/Ti_2C(OH)_2$ atop-I. The potential drop ΔV_∞ across the vacuum is shown. The interface position is indicated by the vertical dashed line.

In conclusion, we have studied three kinds of interfaces, MoS_2/Ti_2C, MoS_2/Ti_2CF_2, and $MoS_2/Ti_2C(OH)_2$, which can be divided into two classes according to the calculated energetics. Strong chemical bonds form in MoS_2/Ti_2C, while a much weaker interaction (that is not sensitive to the specific geometry) is found in the latter two interfaces. The metal-induced states significantly modify the electronic structure of MoS_2 in the case of MoS_2/Ti_2C. The fact that a metallic character emerges shows that deposition of Ti_2C on MoS_2 can lead to conductive MoS_2. In both the MoS_2/Ti_2CF_2 and $MoS_2/Ti_2C(OH)_2$ interfaces, the semiconducting nature is preserved for the physisorbed MoS_2. The bond alignment implies weak and strong n-type doping of the MoS_2 in MoS_2/Ti_2CF_2 and $MoS_2/Ti_2C(OH)_2$ with corresponding n-type Schottky barrier heights of 0.85 and 0.26 eV. The MoS_2/Ti_2CF_2 interface is found to be close to the Schottky limit with negligible charge transfer at the interface. At the $MoS_2/Ti_2C(OH)_2$ interface, a 2.50 eV discontinuity between the vacuum levels on the two sides of the interface indicates that the barrier in this case is mainly due to the interface dipole induced by charge rearrangement.

---

*Corresponding author: udo.schwingenschlogl@kaust.edu.sa

[1] B. Radisavljevic, A. Radenovic, J. Brivio, V. Giacometti, and A. Kis, Nature Nanotech. **6**, 147 (2011).
[2] Z. Yin, H. Li, H. Li, L. Jiang, Y. Shi, Y. Sun, G. Lu, Q. Zhang, X. Chen, and H. Zhang, ACS Nano **6**, 74 (2011).
[3] G. Eda, T. Fujita, H. Yamaguchi, D. Voiry, M. Chen, and M. Chhowalla, ACS Nano **6**, 7311 (2012).
[4] Y. Wu, J. Xiang, C. Yang, W. Lu, and C. M. Lieber, Nature **430**, 61 (2004).
[5] I. Popov, G. Seifert, and D. Tománek, Phys. Rev. Lett. **108**, 156802 (2012).
[6] L. Britnell, R. V. Gorbachev, R. Jalil, B. D. Belle, F. Schedin, A. Mishchenko, T. Georgiou, M. I. Katsnelson, L. Eaves, S. V. Morozov, N. M. R. Peres, J. Leist, A. K. Geim, K. S. Novoselov, and L. A. Ponomarenko, Science **335**, 947 (2012).
[7] Q. H. Wang, K. Kalantar-Zadeh, A. Kis, J. N. Coleman, and M. S. Strano, Nature Nanotech. **7**, 699 (2012).
[8] D. Xiao, G.-B. Liu, W. Feng, X. Xu, and W. Yao, Phys. Rev. Lett. **108**, 196802 (2012).
[9] S. Bertolazzi, J. Brivio, and A. Kis, ACS Nano **5**, 9703 (2011).
[10] A. Castellanos-Gomez, M. Poot, G. A. Steele, H. S. J. van der Zant, N. Agraït, and G. Rubio-Bollinger, Adv. Mater. **24**, 772 (2012).
[11] T. Li, Phys. Rev. B **85**, 235407 (2012).
[12] A. Splendiani, L. Sun, Y. Zhang, T. Li, J. Kim, C.-Y. Chim, G. Galli, and F. Wang, Nano Lett. **10**, 1271 (2010).
[13] G. Eda, H. Yamaguchi, D. Voiry, T. Fujita, M. Chen, and M. Chhowalla, Nano Lett. **11**, 5111 (2011).
[14] K. F. Mak, C. Lee, J. Hone, J. Shan, and T. F. Heinz, Phys. Rev. Lett. **105**, 136805 (2010).
[15] C. Ataca and S. Ciraci, Phys. Rev. B **85**, 195410 (2012).
[16] T. Cao, G. Wang, W. Han, H. Ye, C. Zhu, J. Shi, Q. Niu, P. Tan, E. Wang, B. Liu, and J. Feng, Nature Commun. **3**, 887 (2012).
[17] T. F. Jaramillo, K. P. Jorgensen, J. Bonde, J. H. Nielsen, S. Horch, and I. Chorkendorff, Science **317**, 100 (2007).
[18] Q. Xiang, J. Yu, and M. Jaroniec, J. Am. Chem. Soc. **134**, 6575 (2012).
[19] Y. Yoon, K. Ganapathi, and S. Salahuddin, Nano Lett. **11**, 3768 (2011).
[20] Y. Li, H. Wang, L. Xie, Y. Liang, G. Hong, and H. Dai, J. Am. Chem. Soc. **133**, 7296 (2011).

[21]K. Chang and W. Chen, Chem. Commun. **47**, 4252 (2011).
[22]C. R. Dean, A. F. Young, I. Meric, C. Lee, L. Wang, S. Sorgenfrei, K. Watanabe, T. Taniguchi, P. Kim, K. L. Shepard, and J. Hone, Nat. Nano **5**, 722 (2010).
[23]G. Giovannetti, P. A. Khomyakov, G. Brocks, P. J. Kelly, and J. van den Brink, Phys. Rev. B **76**, 073103 (2007).
[24]J. Slawińska, I. Zasada, and Z. Klusek, Phys. Rev. B **81**, 155433 (2010).
[25]J. N. Coleman *et al.*, Science **331**, 568 (2011).
[26]M. Naguib, M. Kurtoglu, V. Presser, J. Lu, J. Niu, M. Heon, L. Hultman, Y. Gogotsi, and M. W. Barsoum, Adv. Matter. **23**, 4248 (2011).
[27]M. Naguib, O. Mashtalir, J. Carle, V. Presser, J. Lu, L. Hultman, Y. Gogotsi, and M. W. Barsoum, ACS Nano **6**, 1322 (2012).
[28]Q. Tang, Z. Zhou, and P. Shen, J. Am. Chem. Soc. **134**, 16909 (2012).
[29]M. Naguib, J. Come, B. Dyatkin, V. Presser, P.-L. Taberna, P. Simon, M. W. Barsoum, and Y. Gogotsi, Electrochem. Commun. **16**, 61 (2012).
[30]L.-Y. Gan, D. Huang, and U. Schwingenschlögl (submitted).
[31]D. Yang, S. J. Sandoval, W. M. R. Divigalpitiya, J. C. Irwin, and R. F. Frindt, Phys. Rev. B **43**, 12053 (1991).
[32]A. Molina-Sánchez and L. Wirtz, Phys. Rev. B **84**, 155413 (2011).
[33]A. N. Enyashin and A. L. Ivanovskii, Comput. Theor. Chem. **989**, 27 (2012).
[34]G. Kresse and J. Hafner, Phys. Rev. B **47**, 558 (1993).
[35]G. Kresse and J. Hafner, Phys. Rev. B **48**, 13115 (1993).
[36]G. Kresse and J. Furthmüller, Comput. Mater. Sci. **6**, 15 (1996).
[37]G. Kresse and J. Furthmüller, Phys. Rev. B **54**, 11169 (1996).
[38]J. P. Perdew, K. Burke, and M. Ernzerhof, Phys. Rev. Lett. **77**, 3865 (1996).
[39]S. Grimme, J. Comput. Chem. **27**, 1787 (2006).
[40]The value has been carefully tested with respect to the thickness of the vacuum. The absolute difference is less than 10 meV as the thickness is increased to 40 Å. Additionally, all the work functions are calculated using a vacuum of 40 Å.
[41]Y. Ma, Y. Dai, M. Guo, C. Niu, and B. Huang, Nanoscale **3**, 3883 (2011).
[42]G. Giovannetti, P. A. Khomyakov, G. Brocks, V. M. Karpan, J. van den Brink, and P. J. Kelly, Phys. Rev. Lett. **101**, 026803 (2008).
[43]P. A. Khomyakov, G. Giovannetti, P. C. Rusu, G. Brocks, J. van den Brink, P. J. Kelly, Phys. Rev. B **79**, 195425 (2009).
[44]J. Tersoff, Phys. Rev. Lett. **52**, 465 (1984).
[45]E. Shustorovich and H. Sellers, Surf. Sci. Rep. **31**, 5 (1998).
[46]E. Scalise, M. Houssa, G. Pourtois, V. V. Afanas'ev, and A. Stesmans, Nano Research **5**, 43 (2012).
[47]W. Chen, E. J. G. Santos, W. Zhu, E. Kaxiras, and Z. Zhang, Nano Lett. **13**, 509 (2013).
[48]J. Robertson, J. Vac. Sci. Technol. B **18**, 1785 (2000).
[49]R. T. Tung, Phys. Rev. B **64**, 205310 (2001).
[50]R. T. Tung, Phys. Rev. Lett. **84**, 6078 (2000).